Characterization of Endostatin Binding to Heparin and Heparan Sulfate by Surface Plasmon Resonance and Molecular Modeling Role of Divalent Cations

THE JOURNAL OF BIOLOGICAL CHEMISTRY
Vol. 279, No. 4, Issue of January 23, pp. 2927–2936, 2004

Printed in U.S.A.

Characterization of Endostatin Binding to Heparin and Heparan Sulfate by Surface Plasmon Resonance and Molecular Modeling

ROLE OF DIVALENT CATIONS*

Received for publication, September 5, 2003, and in revised form, October 22, 2003
Published, JBC Papers in Press, October 28, 2003, DOI 10.1074/jbc.M309868200

Sylvie Ricard-Blum‡§, Olivier Féraud¶, Hugues Lortat-Jacob‡, Anna Rencurosi‖, Naomi Fukai, Fatima Dkhissi‡‡, Daniel Vittet¶, Anne Imberty‖, Bjorn R. Olsen**, and Michel van der Rest¶**

*From the ‡Institut de Biologie Structurale CEA-CNRS-UJF, UMR 5075, 41 rue Jules Horowitz, 38027 Grenoble Cedex 01, France, ¶Departement Reponse et Dynamique Cellulaires, Commissariat à l'Energie Atomique, 17 rue des Martyrs, 38054 Grenoble Cedex 9, France, ‖Centre de Recherches sur les Macromolecules Vegetales, Domaine Universitaire, 601 Rue de la Chimie, BP 53, 38041 Grenoble Cedex 9, France, **Department of Cell Biology, Harvard Medical School, Boston, Massachusetts 02115, and ‡‡INSERM U553, Hôpital Saint-Louis, 1 avenue Claude Vellefeaux, 75475 Paris Cedex 10, France*

Endostatin (20 kDa) is a C-terminal proteolytic fragment of collagen XVIII that is localized in vascular basement membrane zones in various organs. It binds zinc, heparin/heparan sulfate, laminin, and sulfatides and inhibits angiogenesis and tumor growth. Here we determined the kinetics and affinity of the interaction of endostatin with heparin/heparan sulfate and investigated the effects of divalent cations on these interactions and on the biological activities of endostatin. The binding of human recombinant endostatin to heparin and heparan sulfate was studied by surface plasmon resonance using BIAcore technology and further characterized by docking and molecular dynamics simulations. Kinetic data, evaluated using a 1:1 interaction model, showed that heparan sulfate bound to and dissociated from endostatin faster than heparin and that endostatin bound to heparin and heparan sulfate with a moderate affinity ($K_D \sim 2\ \mu M$). Molecular modeling of the complex between endostatin and heparin oligosaccharides predicted that, compared with mutagenesis studies, two further arginine residues, Arg^{47} and Arg^{66}, participated in the binding. The binding of endostatin to heparin and heparan sulfate required the presence of divalent cations. The addition of $ZnCl_2$ to endostatin enhanced its binding to heparan sulfate by ~40% as well as its antiproliferative effect on endothelial cells stimulated by fibroblast growth factor-2, suggesting that this activity is mediated by the binding of endostatin to heparan sulfate. In contrast, no increase in the anti-angiogenic and anti-proliferative activities of endostatin promoted by vascular endothelial growth factor was observed upon the addition of zinc.

Endostatin (20 kDa), first identified by O'Reilly *et al.* (1), is a proteolytic fragment from the C-terminal domain of collagen XVIII. It inhibits tumor angiogenesis by interfering at several levels with growth factor signaling (2). Two heparin-binding sites have been identified in endostatin involving two clusters of arginine residues, and a zinc binding site is located in the N-terminal part of the molecule (see Refs. 3–5 for reviews). The possibility that its anti-angiogenic effect might be related to displacement of angiogenic factors from the surface of endothelial cells through binding of heparan sulfate has prompted several investigations of its interaction with heparin and heparan sulfate (6–10). The role of zinc in the biological activity of endostatin remains controversial. Zinc binding has been reported to be essential for the anti-angiogenic activity of endostatin (11). Indeed, mutations of amino acids involved in zinc coordination to alanines significantly reduce its anti-tumoral activity, the mutants being unable to cause regression of Lewis lung carcinoma (11). On the other hand, zinc binding does not appear to be critical for the inhibitory effects of endostatin on VEGF[1]-induced migration and tumor growth in mice (12). However, it is of crucial importance to determine the co-factors, if any, that participate in the binding of endostatin to heparin, because heparin binding is required for the inhibition of FGF-2-induced angiogenesis in the chicken chorioallantoic membrane (7, 13), for the activation of tyrosine kinase activity and Shb-induced apoptosis of endothelial cells (13).

The aim of this work was to study the interactions of endostatin with heparin and its physiological ligand, heparan sulfate, to (i) determine the affinity of these interactions and the corresponding interaction models by performing surface plasmon resonance (SPR) kinetic analysis, (ii) identify the structural features of heparin and heparan sulfate participating in the binding to endostatin using SPR binding assays and molecular modeling, and (iii) investigate the effect of divalent cations on the interaction of endostatin with heparin/heparan sulfate and on its anti-angiogenic and anti-proliferative activities *in vitro*.

EXPERIMENTAL PROCEDURES

Production and Purification of Human Endostatin—Recombinant human endostatin was produced by human embryonic kidney cells expressing Epstein-Barr virus nuclear antigen (293-EBNA cells). A construct was generated for expression of endostatin with the oligopeptide epitope of influenza virus hemagglutinin (*flag*) at the N-terminal end (12). The conditioned culture medium was filtered through 0.22-μm filters and applied to a Hi-Trap heparin column (5 ml, Amersham Biosciences) equilibrated in 20 mM Tris-HCl buffer, pH 7.5, containing

* This work was supported by Grant 5783 from the Association pour la Recherche sur le Cancer (to M. v. d. R.) and by National Institutes of Health Grant AR36820 (to B. R. O.). The costs of publication of this article were defrayed in part by the payment of page charges. This article must therefore be hereby marked "*advertisement*" in accordance with 18 U.S.C. Section 1734 solely to indicate this fact.

§ To whom correspondence should be addressed. Tel.: 33-4-38-78-23-90; Fax: 33-4-38-78-54-94; E-mail: ricard@ibs.fr.

[1] The abbreviations used are: VEGF, vascular endothelial growth factor; FGF-2, fibroblast growth factor-2; IMDM, Iscove's modified Dulbecco's medium; RU, resonance unit; SPR, surface plasmon resonance; EBNA, Epstein-Barr virus nuclear antigen; PIM, Perez Imberty Meyer.

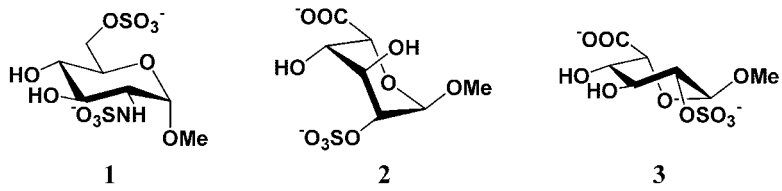

FIG. 1. **Three sulfated monosaccharides.** Methyl-*O*-(2-deoxy-2-*N*-sulfo-3,6-di-*O*-sulfo)-α-D-glucopyranoside (**1**) and methyl-*O*-(2-*O*-sulfo)-α-L-idupyranosuronate in its $^1C_4$ and ^2SO shapes (**2** and **3**) were considered for docking.

0.15 M NaCl. Endostatin was eluted by a linear gradient of NaCl concentration from 0.15 to 1 M and further purified by gel filtration on a Superdex S75 column (2.6 × 60 cm, Amersham Biosciences) in phosphate-buffered saline, pH 7.4 (Sigma). Purified endostatin was concentrated by ultrafiltration and stored at −20 °C. Recombinant human endostatin produced in *Pichia pastoris* was used as well as endostatin commercially available from Calbiochem.

Surface Plasmon Resonance Binding Assays Using BIAcore Technology—The SPR measurements were performed on a BIAcore Upgrade and on a BIAcore 3000 instruments (BIAcore AB, Uppsala, Sweden). Streptavidin (100 μg/ml in 10 mM acetate buffer, pH 4.0) was covalently immobilized to the dextran matrix of an F1 sensor chip via its primary amine groups (amine coupling kit, BIAcore AB) at a flow rate of 5 μl/min. Activation and blocking steps were performed as described previously (14). Streptavidin surfaces were used to capture biotinylated heparin and heparan sulfate. Heparin (from porcine intestinal mucosa, 16 kDa, Sigma) and heparan sulfate (from porcine intestinal mucosa, Celsus, Cincinnati, OH) were biotinylated at their reducing ends (15) and injected over streptavidin in 10 mM Hepes, pH 7.4, 0.3 M NaCl, and 0.005% P20 surfactant at a flow rate of 10 μl/min. An immobilization level ranging between 70 and 200 resonance units (RU) was obtained. A control flow cell was prepared by immobilizing only streptavidin. Control sensorgrams were automatically subtracted from the sensorgrams obtained with immobilized heparin or heparan sulfate to yield true binding responses (14).

Binding assays were performed at 25 °C in 10 mM Hepes buffer, pH 7.4, containing 0.15 M NaCl and 0.005% (v/v) P20 surfactant (HBS-P buffer, BIAcore AB). Endostatin was dialyzed against this buffer and injected at several concentrations and different flow rates over immobilized glycosaminoglycans. The surface was then regenerated with a pulse of 1 M sodium chloride. The kinetic parameters k_a and k_d (association and dissociation rate constants, respectively) were analyzed simultaneously using a global data analysis program (BIAevaluation 3.1 software). This software also fitted simultaneously the sensorgrams obtained at different concentrations of endostatin, constraining the kinetic rate constants to a single value for each set of curves. Apparent equilibrium dissociation constants (K_D) were calculated as the ratio of k_d/k_a. R_{max}, the maximal capacity of the surface was floated during the fitting procedure. The χ^2 value is a standard statistical measure of the closeness of fit. It represents the mean square of the signal noise (BIAevaluation 3.0, Software Handbook).

Heparin and Heparan Sulfate Oligosaccharides and Desulfated Heparins—Heparin oligosaccharides of a defined size were prepared by digestion of heparin with heparinase I followed by gel filtration chromatography on a Bio-Gel P-10 column (16). Heparan sulfate oligosaccharides were prepared by digestion of heparan sulfate by heparinase III. Selectively desulfated heparins were kindly provided by Prof. John Gallagher (Paterson Institute for Cancer Research, Christie Hospital National Health Service Trust, Manchester, UK). Heparin initially contained 97.7% of the *N*-sulfate groups, 89.3% of the 2-*O*-sulfate groups, and 92.4% of the 6-*O*-sulfate groups. De-*N*-sulfated/re-*N*-acetylated heparin contained 90.5% of the 2-*O*-sulfate groups, 85.3% of the 6-*O*-sulfates, and a very low amount of remaining *N*-sulfate groups (2.4%). De-2-*O*-sulfated heparin contained 80.2% of the 6-*O*-sulfate groups, 91.4% of the *N*-sulfate groups, and a residual 2.2% of the 2-*O*-sulfates. De-6-*O*-sulfated heparin contained 98.2% of the *N*-sulfate groups, 54.7% of the 2-*O*-sulfate groups, and a residual 4.2% of the 6-*O*-sulfates (17). De-*O*-sulfated heparin contained 91.6% of the *N*-sulfates, 7.1% of the 2-*O*-sulfates, and 3.6% of the 6-*O*-sulfates.

Docking Calculations—The starting model of human endostatin was made from the crystal structure of the monomer (18) taken from the Protein Data Bank (code 1BNL) (19). All graphical editions were performed with the SYBYL package (Tripos Inc., St Louis, MO). Hydrogen atoms were added to the protein, and Connolly surfaces were calculated using the MOLCAD program (20).

Monosaccharide Docking—Docking of monosaccharide was performed using the AutoDock 3.0 program (21). AMBER force field charges were assigned to all protein atoms. Because no parameter exists for the zinc atom, it was not considered in the calculations. During an AutoDock 3.0 simulation, multiple Lamarckian Genetic Algorithm runs occurred, each one providing one solution (*i.e.* one predicted binding mode), and cluster analysis was performed at the end of the simulation. Solutions that were within a 1-Å root-mean-square deviation of each other belonged to the same cluster, and the clusters were ranked according to their lowest energy member. A dielectric constant of 4 r was selected for the calculations because water molecules are almost excluded from the interface between the protein and the charged monosaccharide. Three sulfated monosaccharides, *i.e.* methyl-*O*-(2-deoxy-2-*N*-sulfo-6-mono)-α-D-glucopyranoside (Fig. 1, **1**) and the methyl-*O*-(2-*O*-sulfo)-α-L-idupyranosuronate in its $^1C_4$ and ^2SO shape (Fig. 1, **2** and **3**), were considered for docking. Atomic coordinates for the sulfated monosaccharides were extracted from a data bank of the three-dimensional structures (infopc2.cermav.cnrs.fr/data bank/monosaccharides/), and partial charges were assigned to the atoms according to the PIM force field (16, 22). Grids of probe atom interaction energies and electrostatic potential were generated around the whole protein using the AutoGrid program present in AutoDock 3.0 with a spacing of 0.5 Å. All probes were placed arbitrarily at a distance of 10 Å from the protein surface, and their rotatable torsion angles were allowed to rotate freely. For each monosaccharide one job of 100 docking runs was performed using a population of 200 individuals and an energy evaluation number of 2×10^6.

Decasaccharide Docking—The structures of two heparin decamers that differ in the conformation of the iduronate residue ($^1C_4$ or ^2SO) were extracted from the Protein Data Bank (code 1HPN) (23). Partial charges were assigned as described above. Because of the limitation of the docking program, the docking was performed using a rigid body approach, and the largest possible ligand that could be considered was a decasaccharide. This ligand was placed 10 Å away from the surface of the protein, in a 30 × 46.5 × 46.5-Å box with 0.375-Å grid spacing, covering the putative binding site surface. For each decasaccharide, one job of 100 runs was performed using a population of 200 individuals and an energy evaluation number of 3×10^6.

Molecular Dynamics Simulation—To introduce some flexibility into the system a 200 ps molecular dynamics on the protein-heparin complex was performed at 300 K. The TRIPOS force field (24) was used with Pullman partial charges assigned to the protein. PIM parameters especially developed for these types of sugars (16, 22) were employed for the heparin oligosaccharide. The protein backbone was kept fixed during the simulation. The molecular dynamics simulation was ended by a 30-ps simulated annealing process at 50 K, to pull the complex into a low energy conformation. The starting complex structures were derived from the lowest energy docked conformers. Two molecular dynamics simulations were performed using heparin oligosaccharide with the reducing end in opposite orientations.

Sprouting Angiogenesis from Embryonic Stem Cell-derived Embryoid Body Secondary Cultures into Type I Collagen Gels—Embryonic stem cells, line CJ7, were induced to differentiate in a semi-solid methylcellulose medium as described previously (25, 26). For secondary culture into collagen gel, 11-day-old embryoid bodies were collected by diluting the medium with IMDM Glutamax. After low speed centrifugation (180 × *g*, 5 min) and two further washes, embryoid bodies were suspended in fresh IMDM Glutamax and mixed with a collagen-containing culture medium at a final concentration of 50 embryoid bodies/ml, and 1.2 ml were poured into a 35-mm bacterial grade Petri dish (27). The final composition of the collagen-based culture medium was as follows: IMDM containing 1.25 mg/ml rat tail type I collagen (BD Biosciences), 15% fetal calf serum, 450 μM monothioglycerol, 10 μg/ml insulin, 50 units/ml penicillin, and 50 μg/ml streptomycin (27). Cultures were performed in the presence of 15 ng/ml VEGF (Peprotech, Rocky Hill,

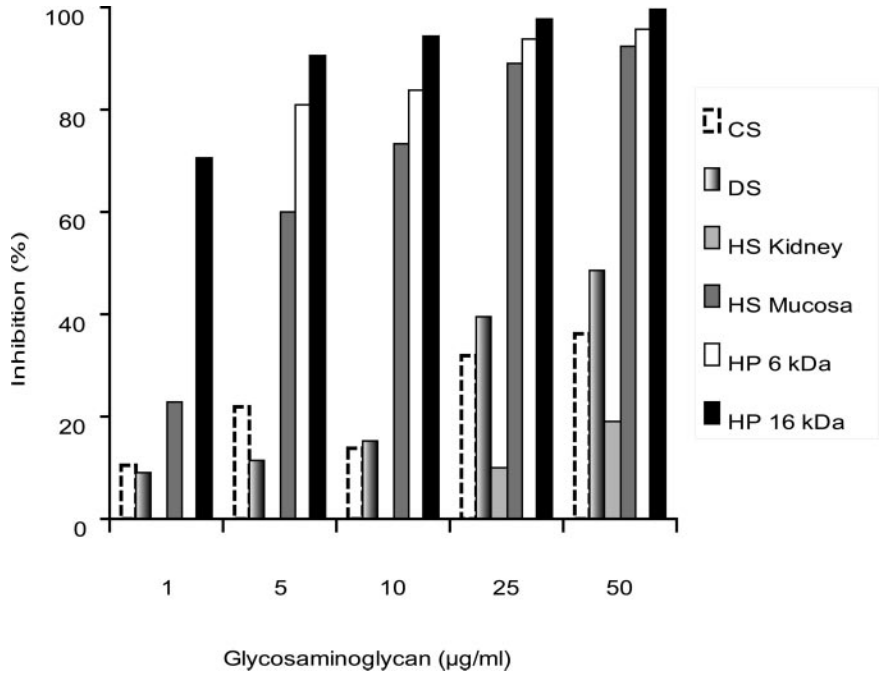

FIG. 2. **Inhibition of the binding of recombinant human endostatin (5 μM, *P. pastoris*) to heparin by different glycosaminoglycans.** Endostatin was incubated at room temperature for 1 h with different concentrations of glycosaminoglycans and then was injected over immobilized heparin (*HP*) (101 RU; flow rate, 15 μl/min; injected volume, 60 μl). Two sources of heparan sulfate (*HS*) (bovine kidney from Sigma and porcine intestinal mucosa from Celsus) were used. *CS*, chondroitin sulfate; *DS*, dermatan sulfate.

NJ). Embryoid bodies were first preincubated with endostatin (10 μg/ml) for 1 h at 37 °C in IMDM before being seeded into collagen medium containing VEGF. Quantitative analysis of sprouting angiogenesis was performed 3 days after secondary plating by computer-assisted morphometric analysis, after prior revelation of endothelial cells by CD31 immunostaining experiments (27).

Cell Proliferation Assays—The effect of endostatin on cell proliferation was tested on human umbilical vein endothelial cells stimulated by 10 ng/ml VEGF or 10 ng/ml FGF-2 as well as on the following cell lines: human colon adenocarcinoma cell line HT29, murine colon adenocarcinoma cell line C51, and human breast cancer cell line MDA-MB-231. Cells were grown in 96-well tissue culture plate (4×10^4 cells/well) for 24 h in a complete culture medium. The serum was then removed for 24 h before incubating the cells with 5 μg/ml endostatin in the presence or absence of 50 μM zinc chloride for 72 h. Cell proliferation was quantitated by a colorimetric cell proliferation assay containing a tetrazolium compound (Promega).

RESULTS

Inhibition of Endostatin Binding to Heparin and Heparan Sulfate by Glycosaminoglycans—SPR binding assays confirmed that human recombinant endostatin from *P. pastoris* bound to immobilized heparin. This binding was strongly inhibited by heparin and to a lesser extent by dermatan sulfate from porcine intestinal mucosa and by chondroitin sulfate from bovine trachea (Fig. 2). No significant difference in inhibition was observed for heparin with different molecular masses (6 and 16 kDa). Heparan sulfate from bovine kidney was a very poor inhibitor compared with heparin, which inhibited 70% of the interaction at a concentration of 1 μg/ml. In contrast, heparan sulfate from porcine intestinal mucosa strongly inhibited the binding of endostatin to immobilized heparin (Fig. 2) and heparan sulfate (data not shown).

Binding of Heparin and Heparan Sulfate Oligosaccharides to Endostatin—Heparin and heparan sulfate oligosaccharides were used to evaluate the minimum size of these two glycosaminoglycans required for endostatin binding using SPR inhibition experiments. The binding of endostatin to heparin or heparan sulfate increased with increasing length of heparin and heparan sulfate oligosaccharides (data not shown). The smallest size of heparin showing at least 50% inhibition of binding was a 12-mer oligosaccharide, whereas a longer oligosaccharide of heparan sulfate (16-mer) was required to achieve a similar level of inhibition. No significant inhibition was observed with the short heparan sulfate oligosaccharides (6- and 8-mer), whereas the heparin oligosaccharides of the same size inhibited endostatin binding to heparin by 22 and 34%, respectively, and to heparan sulfate by 14 and 21%. The inhibition by heparin and heparan sulfate oligosaccharides of endostatin binding to heparan sulfate was stronger than the inhibition of endostatin binding to heparin.

N-Sulfation and 2-O-Sulfation of Heparin Are Involved in the Binding to Endostatin—Inhibition experiments were carried out with selectively desulfated heparins to identify the sulfate groups of heparin participating in the interaction with endostatin. Desulfated heparins were incubated for one h with endostatin before injection over heparin (Fig. 3*A*) or heparan sulfate (Fig. 3*B*). If a particular desulfated heparin retained its ability to interact with endostatin, the injection of the complex resulted in inhibition of endostatin binding to immobilized heparin or heparan sulfate. In this experimental set-up, a strong inhibition indicated that the removed sulfate groups were not involved in the binding. *N*-sulfation contributed the most to the binding of endostatin. The contribution of 2-*O*-sulfation to endostatin binding was also significant, whereas that of 6-*O*-desulfation was less.

Endostatin Binds to Heparin and Heparan Sulfate with a Moderate Affinity—Kinetic analysis was performed by injecting different concentrations of endostatin either over immobilized heparan sulfate (Fig. 4) or heparin (data not shown). The dissociation rate of the complexes of endostatin with heparin or heparan sulfate was not influenced by the contact time (from 4 up to 8 min, data not shown). According to kinetic analysis using BIAevaluation software, two interaction models could account for the mechanism of endostatin binding to glycosaminoglycans: a 1:1 Langmuir model or a heterogeneous ligand model involving parallel reactions of each immobilized glycosaminoglycan with endostatin. The addition of a term that takes mass transfer into account did not improve the fitting of the experimental data. Mass transfer was thus not considered as a limitation for the evaluation of kinetic parameters.

Human recombinant endostatin from *P. pastoris* bound to heparan sulfate with a moderate affinity. The affinity constant K_D was found to be 2.2 μM using the 1:1 Langmuir model to fit the data (χ^2 5.06). The association and dissociation rate con-

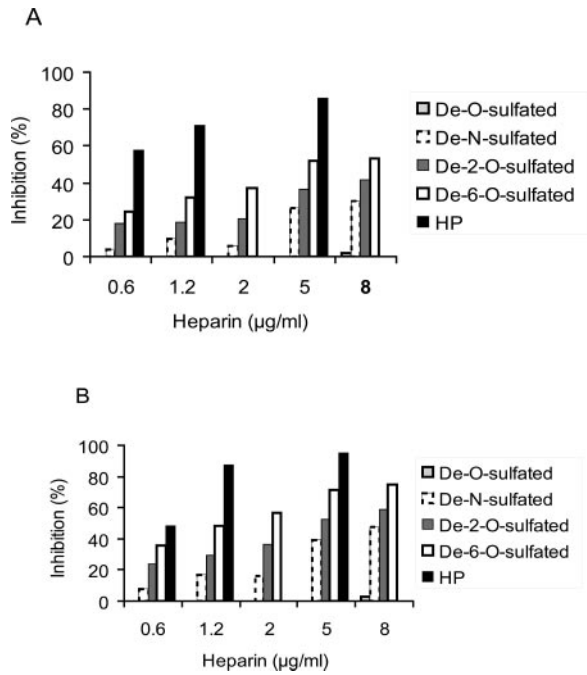

FIG. 3. **Human recombinant endostatin from *P. pastoris* (5 μM) was preincubated with several concentrations of selectively desulfated heparins for 1 h at room temperature before injection over immobilized heparin (117 RU) (*A*) or heparan sulfate (152 RU) (*B*) (flow rate, 15 μl/min; injected volume, 60 μl).**

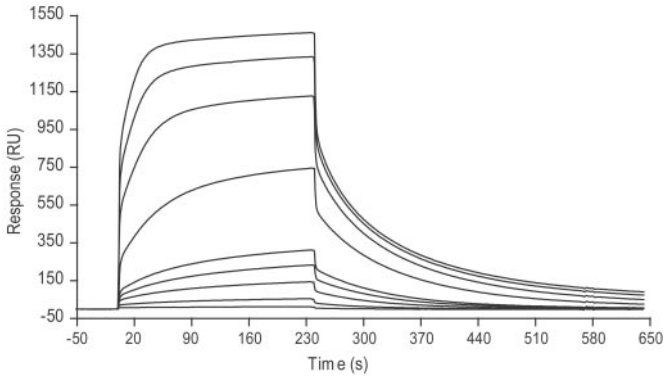

FIG. 4. **Overlay of sensorgrams resulting from the injection of different concentrations (0.2–10 μM) of human recombinant endostatin from *P. pastoris* over immobilized heparan sulfate from porcine intestinal mucosa (96 RU; flow rate, 15 μl/min; injected volume, 60 μl).**

stants were 9.04×10^3 M^{-1} s^{-1} and 19.9×10^{-3} s^{-1}, respectively. A similar affinity was obtained for the interaction between endostatin and heparin (K_D 1.96 μM, 1:1 Langmuir model, χ^2 7.23), but the kinetic parameters were different, 2.23×10^3 M^{-1} s^{-1} for k_a and 4.35×10^{-3} s^{-1} for k_d. Heparan sulfate formed a kinetically weaker complex than heparin with endostatin, as shown by the faster dissociation rate. Binding data to heparin and heparan sulfate were also well fitted to the heterogeneous ligand model predefined in the BIAeval 3.1 software, which included the effects of possible heterogeneity of immobilized glycosaminoglycans. In this model, endostatin could bind to two sites via parallel reactions on immobilized heparin or heparan sulfate. The two sets of calculated affinity constants were: K_{D1}, 0.96 μM, and K_{D2}, 19.84 μM, for heparin (χ^2 2.79); K_{D1}, 1.37 μM, and K_{D2}, 25.25 μM, for heparan sulfate (χ^2 4.82). The highest affinity was in the same range as the values obtained when data were fitted to the 1:1 Langmuir model.

Attempts were made to evaluate the affinity of the interaction between endostatin produced in 293-EBNA cells and heparin or heparan sulfate in the absence of zinc. In both cases, binding data exhibited a good fit to the heterogeneous ligand model, but the affinity was very poor (K_{D1}, 452 μM, and K_{D2}, 68 μM, (χ^2 0.358) for heparan sulfate; K_{D1}, 40 μM, and K_{D2}, 65 μM (χ^2 1.67) for heparin).

Molecular Modeling of Endostatin-Heparin Interactions: Docking of Monosaccharides—Docking studies with heparin monosaccharides and oligosaccharides and endostatin provided additional structural information regarding the interaction. When docking the three sulfated monosaccharides on the endostatin monomer, a large number of clusters was obtained: 47 for monosaccharide **1**, 29 for monosaccharide **2**, and 31 for monosaccharide **3**. The monosaccharides representing the lowest energy member of each cluster were superimposed on the accessible surface of the protein. Highly populated binding zones were noticed all along the most positively charged area of the surface for the three monosaccharides (Fig. 5, *A–C*). The docking results were further analyzed by counting the number of hydrogen bonds occurring between docked conformers and amino acids of endostatin (Fig. 6). The amino acids that seemed to be particularly involved in monosaccharide binding through hydrogen bonding were Arg^{27}, Arg^{47}, Arg^{53}, Arg^{63}, Arg^{66}, and Arg^{139} (Table I). They were distributed in two different clusters apart from Arg^{47}, located between the two clusters at the surface of endostatin (Fig. 5*D*).

Decasaccharide Docking—A heparin decasaccharide was used for a rigid body docking on endostatin. This fragment was long enough to bridge the two clusters of basic amino acids previously identified as heparin binding sites (7). Furthermore, this is the limit of the AutoDock 3.0 program in term of ligand size. Docking of heparin decasaccharides on the endostatin surface yielded 10 and 3 clusters for the polysaccharide with iduronate residues in the $^1C_4$ and ^2SO shape, respectively. The solutions were classified according to the orientation of the polysaccharide with respect to the line connecting the two arginine clusters present on the endostatin surface. The results (not shown) were quite different according to the nature of the iduronate conformer present in the chain. For heparin-$^1C_4$, the docked oligosaccharides were almost all aligned with the line connecting the two clusters. In contrast, for heparin-^2SO, the solutions were equally distributed in two orientations, parallel or perpendicular to this line. The oligosaccharides adopting the perpendicular orientation displayed a significantly lower number of contacts with the protein surface than the oligosaccharide adopting the parallel orientation.

Molecular Dynamics Simulations of the Interaction between Endostatin and Heparin—Four starting points were tested for simulated annealing studies. Heparin-$^1C_4$ and heparin-^2SO were tested in the parallel orientation defined above, with the oligosaccharide ends in opposite directions. Preliminary assays demonstrated that conformational transition of some iduronate rings was observed only when the starting conformer was in the ^2SO shape. Heparin $^1C_4$ was therefore not further considered for molecular dynamics simulations. In the two simulations, a global rearrangement of the chain was observed during the first 50 ps of the dynamics. The chains moved toward Arg^{53}, which was not involved in the binding in the starting structures, and in the meantime some iduronate residues converted from the ^2SO to $^1C_4$ conformation. The resulting structure was stable for the remaining 150 ps with the exception of some fluctuations at the extremities of the oligosaccharide that were not constrained by interaction with endostatin. The complexes displayed in Fig. 7 represent optimized structures obtained during the annealing phase for the two dynamics simulations

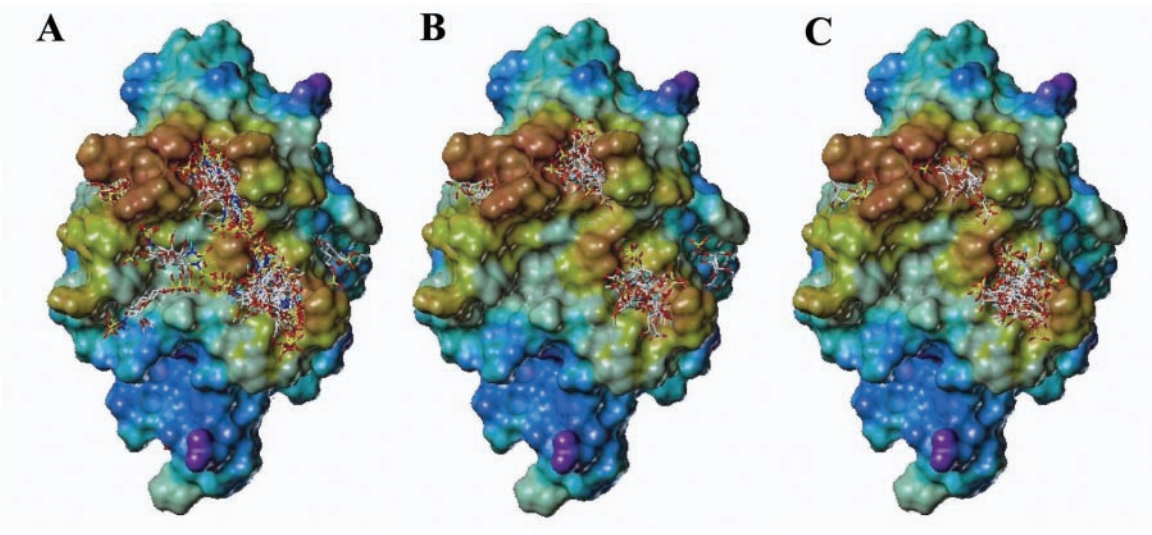

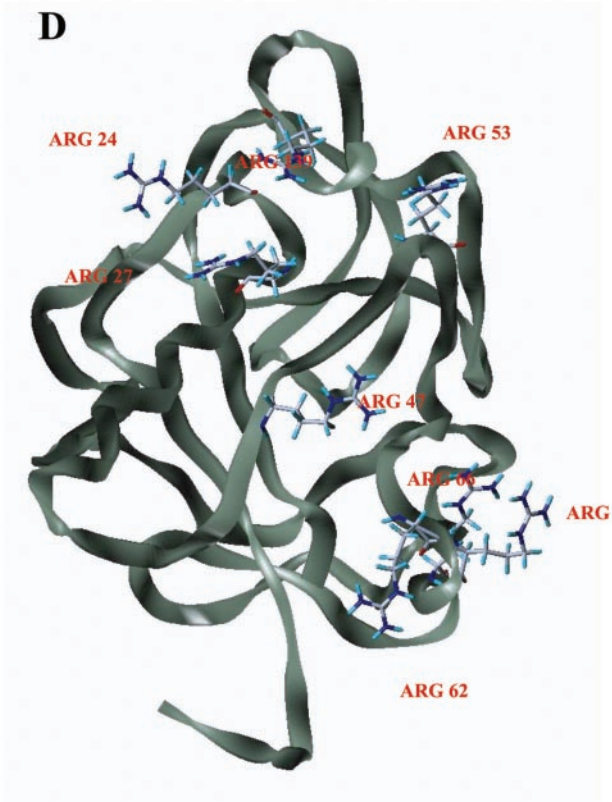

FIG. 5. **Docking prediction for sulfated monosaccharides with human endostatin, which was represented with its Connolly surface color-coded according to the electrostatic potential (from *blue* for negative to *red* for positive areas).** Low energy binding modes were represented for the three monosaccharides, **1** (*A*), **2** (*B*), and **3** (*C*). *D*, ribbon representation of endostatin structure showing the basic amino acids forming basic clusters at the surface of the protein.

with the two possible orientations of the reducing end of the oligosaccharide. In the two models, the heparin chain bridged the two clusters of basic amino acids. The protein surface appeared quite different because the flexible side chains of arginine and lysine residues underwent conformational rearrangement during the molecular dynamics simulation. The binding mode displayed in Fig. 7*A* presented a better fit between the oligosaccharide negative charges and the basic clusters of endostatin. Nevertheless, the occurrence of the binding mode with an inverse polarity of the heparin oligosaccharide (Fig. 7*B*) cannot be ruled out.

The Binding of Endostatin to Heparin and Heparan Sulfate Depends on Divalent Cations—To compare human recombinant endostatin from two different sources, endostatin produced by 293-EBNA cells was also tested for heparin and heparan sulfate binding in the same experimental conditions described above for the analysis of endostatin produced in yeast. In these conditions, endostatin from 293-EBNA cells did not bind or bound weakly to immobilized heparan sulfate (Fig. 8) or heparin (data not shown). The lack of binding might be because of the loss of the biological activity of endostatin from 293-EBNA cells during the purification steps. However, as

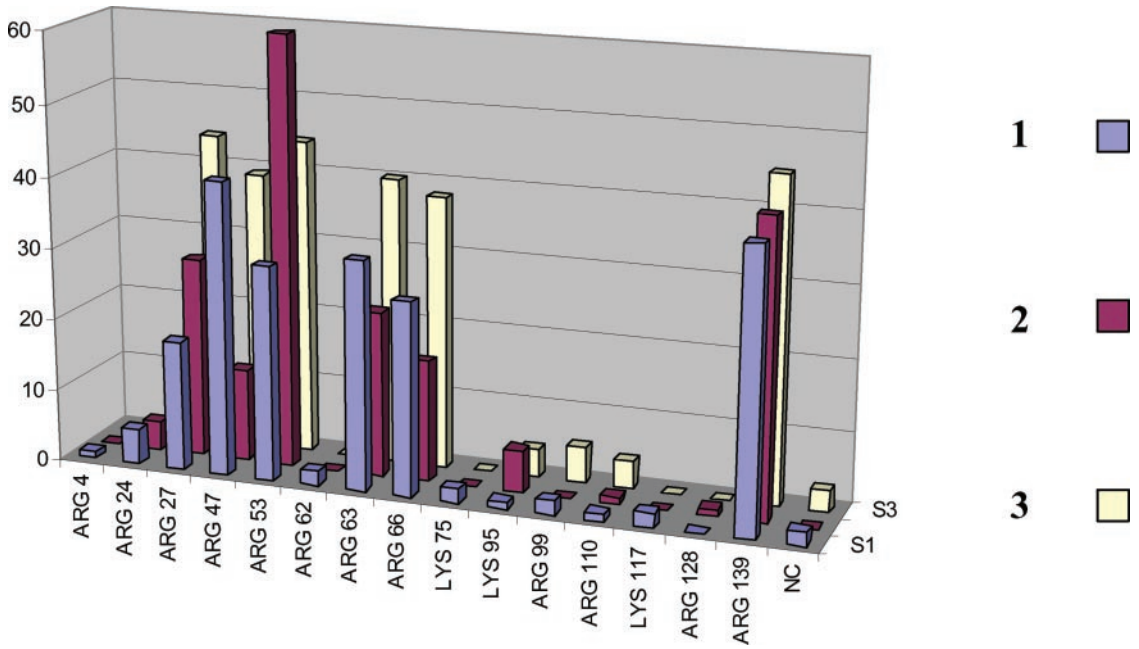

FIG. 6. **Total number of hydrogen bonds predicted to form between sulfated monosaccharides (1, 2, and 3) and basic amino acids of human endostatin during docking simulations.** Arginine residues were *numbered* from the first amino acid residue of human endostatin (His^{1}, also referred to as His^{132} when numbering starts from the first amino acid of the whole C-terminal domain NC1 of collagen XVIII).

TABLE I

Experimental and modeling data on the involvement of the arginine residues of endostatin in its binding to sulfated monosaccharides

Murine endostatin	Mutagenesis[a]	Human endostatin	AutoDock 3.0[b]
	NaCl (M)		*No. of hydrogen bonds*
Wild	0.35		
Arg^{155}	0.25	Arg^{24}	10
Arg^{158}	0.19	Arg^{27}	90
Arg^{169}	0.33	Arg^{38}	0
Arg^{178}	No data	Arg^{47}	93
Arg^{184}	0.25	Arg^{53}	134
Arg^{193} + Arg^{194}	0.27	Arg^{62} + Arg^{63}	2 + 95
Arg^{197}	No data	Arg^{66}	82
Arg^{241}	0.34	Arg^{110}	6
Arg^{259}	0.33	Arg^{128}	1
Arg^{270}	0.19	Arg^{139}	125

[a] NaCl concentration required to elute mutants of murine endostatin from a heparin column (numbering starting with His^{132} as the first residue of murine endostatin).

[b] Total number of hydrogen bonds predicted to occur between the 107 solutions for the docked sulfated monosaccharides **1**, **2**, and **3** and human endostatin (numbering starting from the first histidine residue of endostatin).

reported in the next paragraph, this endostatin inhibited angiogenesis and cell proliferation *in vitro* and was thus biologically active. Another possibility to explain the low binding of the 293-EBNA cell-derived endostatin was the absence of a necessary co-factor. Because endostatin binds one atom of zinc (18), and because conflicting results on the role of zinc in the interaction of endostatin with heparin have been reported (11, 12), we decided to further investigate the role of zinc and other divalent cations in mediating endostatin binding to heparin or heparan sulfate.

The addition of 10 mM EDTA, which chelates several divalent cations including Ca^{2+} and Zn^{2+}, abolished the binding of endostatin from *P. pastoris* to immobilized heparin and heparan sulfate (95.4 and 96.7% inhibition, respectively). The weak binding to heparin and heparan sulfate observed for some preparations of endostatin produced by 293-EBNA cells was also completely abolished by 10 mM EDTA (94.3 and 96.5% inhibition, respectively. The addition of 10 mM EGTA, which is a Ca^{2+} and Mg^{2+} chelator, also abrogated the binding of the two endostatins to heparin and heparan sulfate (more than 95% inhibition). We also tried to perform inhibition experiments using a Zn^{2+} ion chelator, 1,10-phenanthroline, but this compound bound nonspecifically in the SPR assays, and we were unable to obtain any reliable data.

To determine whether the addition of divalent metal ions to endostatin from 293-EBNA cells could restore or increase its binding to heparin or heparan sulfate, we added them in an equimolar concentration to endostatin before its injection over immobilized glycosaminoglycans. The addition of Zn^{2+}, Ca^{2+}, Mg^{2+}, and Mn^{2+} increased the binding of endostatin from 293-EBNA cells to immobilized heparin and heparan sulfate but not to the same extent (Table II). Zinc and manganese were the most potent enhancers, whereas calcium and magnesium had a lesser effect. Binding enhancement was more pronounced for immobilized heparan sulfate than for immobilized heparin. The addition of zinc also increased the binding of endostatin from *P. pastoris* to heparan sulfate, and no significant increase in binding to heparin was observed (Table II). An increase in cation concentration (10 μM) did not have any further significant effect.

Upon the addition of 5 μM zinc chloride to both sources of endostatin, the binding of 293-EBNA endostatin reached 95.7 and 102.6% of the binding of *Pichia* endostatin to heparin and heparan sulfate, respectively. The addition of an equimolar

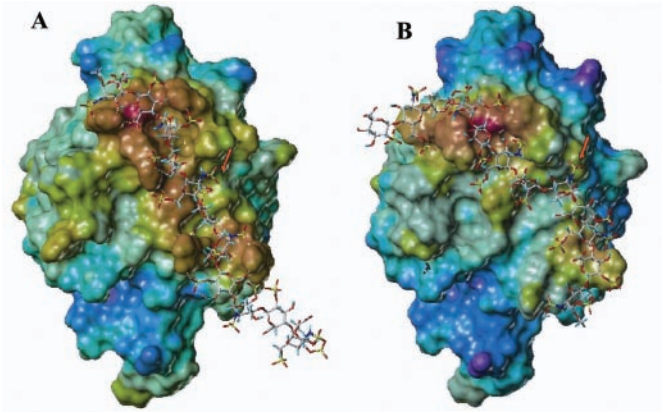

FIG. 7. **Two predicted binding modes of heparin dodecasaccharide with endostatin after simulated annealing.** The two modes differed in the orientation of the polysaccharide chain, with the reducing end at the top (*A*) or at the bottom (*B*). Endostatin is represented as in Fig. 8.

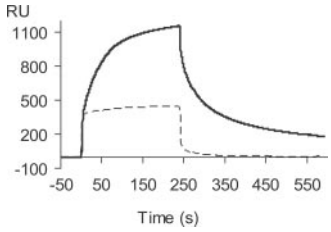

FIG. 8. **Binding of endostatin from *P. pastoris* (——) and of endostatin from 293-EBNA cells (– – –) to immobilized heparan sulfate (215 RU; flow rate, 15 μl/min; injected volume, 60 μl).**

TABLE II

Effect of the addition of several divalent cations to endostatin on its binding to immobilized heparin and heparan sulfate

The results are expressed as percent of increase in binding and were obtained on two different sensor chips (A and B) with different amounts of immobilized heparin and heparan sulfate.

Endostatin	Immobilized heparin	Immobilized heparan sulfate
Pichia pastoris + 5 μM $ZnCl_2$ (A)	5.0	30.0
293-EBNA cells + 5 μM $ZnCl_2$ (A)	30.7	31.8
293-EBNA cells (B)		
+ 5 μM $ZnCl_2$	43.0	51.6
+ 5 μM $CaCl_2$	16.3	23.9
+ 5 μM $MgCl_2$	15.5	22.3
+ 5 μM $MnCl_2$	24.4	35.7

amount of zinc to both preparations of endostatin equalized their binding activities to heparin and heparan sulfate.

The metal ions may bind either heparin (28) or endostatin (18) or both molecules to mediate the enhanced interaction. The injection of 10 mM EDTA on immobilized heparin and heparan sulfate prior to the injection of endostatin did not prevent its binding to the immobilized glycosaminoglycans, suggesting that the divalent cation did not bind to heparin or heparan sulfate but rather was associated with endostatin.

Role of Zinc in the Multimerization of Endostatin—Dimers of endostatin, resistant to SDS, were observed by SDS-PAGE and Western blotting in endostatin from *P. pastoris* and from 293-EBNA cells (data not shown). The multimerization process was observed using SPR assays by injecting endostatin from both sources over immobilized endostatin from *P. pastoris*. The addition of zinc to endostatin prior to its injection increased the interaction of endostatin with itself (Fig. 9).

Effect of Zinc on the Anti-angiogenic Activity of Endostatin—

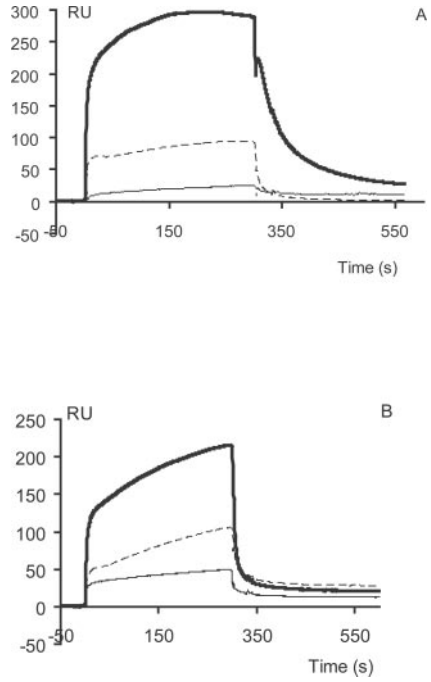

FIG. 9. **Injection of 5 μM human recombinant endostatin from *P. pastoris* (*A*) and 293-EBNA cells (*B*) over immobilized endostatin from *P. pastoris* (2466 RU; flow rate, 20 μl/min; injected volume, 100 μl).** The binding was first recorded in the absence of added zinc (——). Increasing concentrations of zinc at 44 μM (– – –) and 175 μM (——) increased the binding of soluble endostatin to immobilized endostatin.

Using an *in vitro* model of angiogenesis, we evaluated the ability of endostatin generated by *P. pastoris* or by 293-EBNA cells to inhibit endothelial cell sprouting induced by VEGF. Both endostatin preparations significantly decreased the embryoid body endothelial sprouting response elicited by VEGF (Fig. 10). Mean values for the total length of endothelial sprouts per embryoid body were 1426.2 ± 169.2 μm and 948.5 ± 118.8 μm for *P. pastoris* and EBNA-293 endostatins, respectively, and 2138 ± 167.1 μm for the control. Endostatin produced in *P. pastoris* seemed to be less efficient than that from 293-EBNA cells (33.3 and 55.6% inhibition of sprouting, respectively). The mean total embryoid body sprout lengths measured in the presence and absence of 50 μM $ZnCl_2$ (948.5 ± 118.8 μm and 901.7 ± 108.6 μm, respectively) were not significantly different. The addition of zinc did not induce a further inhibition of angiogenesis by endostatin in this model (55.6 and 57.8% inhibition in the absence and presence of zinc chloride, respectively).

Effect of Zinc on the Anti-proliferative Activity of Endostatin—The proliferation of human umbilical vein endothelial cells stimulated by VEGF or by FGF-2 was strongly inhibited by human endostatin from 293-EBNA cells (Table III). When the cells were stimulated by VEGF, the addition of zinc to endostatin resulted in a further decrease in cell proliferation (56.6% inhibition), but this reflected the additive effects of endostatin (43.0%) and zinc (14.6%). The proliferation of cells stimulated by FGF-2 was also further decreased upon the addition of zinc to endostatin (61.7% inhibition) compared with endostatin alone (32.8%). However, and in contrast to the results obtained with VEGF, the increased inhibition of cell proliferation was higher than the combined effect of endostatin and zinc (15.2%).

Endostatin also inhibited the proliferation of a human adenocarcinoma cell line (HT29) by 42.2%. The addition of zinc did not induce a further decrease in cell proliferation (44.8%),

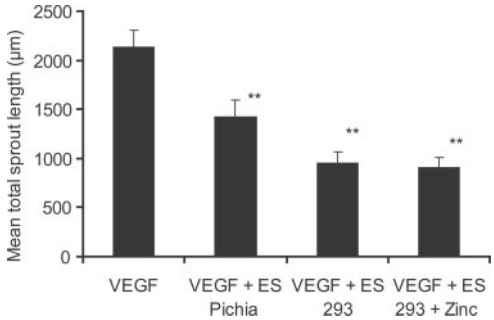

FIG. 10. **Quantitative analysis of endostatin effect on embryoid body endothelial sprouting.** 11-Day-old embryoid bodies were treated with 15 ng/ml VEGF and 10 μg/ml endostatin in the absence or presence of 50 μM $ZnCl_2$. Measurements were performed after 72 h of collagen secondary culture. Data represent mean values ± S.D. (132 embryoid bodies for VEGF alone, 81 for endostatin (Calbiochem), 41 for endostatin from EBNA-293 cells, and 75 for endostatin from EBNA-293 cells with $ZnCl_2$).

TABLE III
Effect of recombinant human endostatin from 293-EBNA cells, with or without added 50 μM zinc chloride, on cell proliferation

The results are expressed as percent of inhibition of proliferation. HUVEC, human umbilical vein endothelial cells; HT29, human colon adenocarcinoma cell line; C51, murine colon adenocarcinoma cell line; MDA-MB-231, human breast cancer cell line.

Cells	Endostatin	Endostatin + $ZnCl_2$	$ZnCl_2$
HUVEC stimulated by VEGF	43.0	56.6	14.6
HUVEC stimulated by FGF-2	32.8	61.7	15.2
HT29	42.2	44.8	24.7
C51	3.1	12.7	11.3
MDA-MB-231	4.2	12.1	13.2

although zinc alone inhibited proliferation by 24.7%. In contrast, recombinant human endostatin had no effect on the proliferation of the MDA-MB-231 murine adenocarcinoma cell line (3.1% inhibition). The combination of endostatin and zinc chloride gave the same inhibition (12.7%) as zinc chloride alone (11.3%).

DISCUSSION

We report here the first detailed kinetic analysis of endostatin binding to heparin and heparan sulfate. Endostatin binds to these glycosaminoglycans with a moderate affinity in the micromolar range. An evaluation of SPR experiments gives further insights into the mechanism governing the interaction. The K_D value calculated by fitting to a Langmuir model using the BIAeval 3.1 software was ~2 μM. This value is consistent with that for endostatin binding to heparin as evaluated by Scatchard analysis ($K_D \sim 0.3$ μM) (7). Heparan sulfate binds to and dissociates from endostatin faster than heparin. The dissociation rate is about 4.5 times higher for heparan sulfate, suggesting that the complex of endostatin with heparan sulfate is more transient in nature than the endostatin-heparin complex. The BIAcore data could also be fitted to a model of ligand heterogeneity involving parallel reactions between immobilized glycosaminoglycans and soluble endostatin. The good fit to this latter model could be explained by the natural heterogeneity of heparin and heparan sulfate. Indeed, heparin and heparan sulfate undergo extensive modifications after the initial polymer synthesis and are thus made up of several domains that could bind endostatin with different affinities.

Heparin oligosaccharides ranging from 6 to 18 monosaccharides in length bound to endostatin, whereas no significant binding to endostatin was observed for the short heparan sulfate oligosaccharides (6- and 8-mer). An oligosaccharide length of heparin greater than a dodecasaccharide size gives optimal binding to endostatin. This is consistent with data obtained using other techniques, which suggest that heparin fragments of 12 or more monosaccharide units are required for efficient binding to endostatin (7). A longer size (16-mer) is required for optimal endostatin binding to its physiological ligand, heparan sulfate. This result, together with the lack of binding of heparan sulfate 6- and 8-mer, support the previous finding that endostatin-bound heparan sulfate oligosaccharides contained predominantly 12–16 mers, a small proportion of 10-mer, and no 8-mer (9).

SPR inhibition assays indicated that *N*-sulfation and 2-*O*-sulfation of heparin are involved in the binding to endostatin. 2-*O*-Sulfation reportedly is crucial for the interaction of heparin with endostatin (7) and is involved in the binding of endostatin to the heparan sulfate chains of glypican (8), although 2-*O*-sulfates have been recently reported by others (10) as not being strictly essential for the interaction of endostatin with heparan sulfate. In SPR inhibition assays, the role of 6-*O*-sulfation of heparin in the binding to endostatin appears to be limited, in contrast to results obtained by affinity chromatography (7) or by a filter binding assay (10).

The protein sequences of human and murine endostatins display 87% identity, and of the 15 arginine residues present in mouse endostatin, all but one are fully conserved in the human protein, the exception being a conservative replacement by lysine (29). Their three-dimensional surfaces are also very similar because superimposition of protein backbones from the crystal structures of the human (18) and mouse (29) proteins yielded a root-mean-square deviation of only 0.50 Å. Results from mutagenesis studies performed on murine endostatin (7) can therefore be compared directly with our model of the human protein for heparin binding properties. Our modeling studies display excellent agreement with experimental data (7) in identifying basic amino acids involved in binding heparin. Arg^{27}, Arg^{53}, Arg^{63}, and Arg^{139} interact more strongly with the docked monosaccharides (Table I), and the corresponding mouse endostatin mutants display a marked lower affinity for heparin (7). Some differences in the binding pattern noticed for the three probes suggest that conformational aspects are relevant. Amino acids reported as not involved in the binding (Arg^{169}, Arg^{241}, and Arg^{259} in murine endostatin) were not identified in human endostatin by the AutoDock program as participating in heparin binding (Arg^{38}, Arg^{110}, and Arg^{128}). Furthermore, two further arginine residues, Arg^{47} and Arg^{66}, for which no mutagenesis data were available, were suggested by the molecular modeling approach to be involved also in the binding of endostatin to heparin. Arg^{66} is located in the vicinity of one of the heparin binding sites (Arg^{62}, Arg^{63}), whereas Arg^{47} is found between the two basic binding sites identified by mutagenesis and could stabilize the interaction. The identification of Arg^{47} and Arg^{66} as residues of endostatin involved in heparin and heparan sulfate binding underlines the key role played by arginine residues in these interactions.

We report here that the binding of endostatin to heparin and heparan sulfate depends upon divalent cations. This requirement for divalent cations was discovered in an effort to understand the lack of binding to heparin and heparan sulfate of highly purified endostatin produced by 293-EBNA cells. A single purification step of affinity chromatography on a HiTrap heparin column of the culture medium of 293-EBNA cells was insufficient to obtain pure endostatin, as demonstrated by the presence in SDS-PAGE of high molecular weight contaminants co-eluted with endostatin from the heparin affinity column. A second step of purification by gel filtration was thus performed, and it is likely that the divalent ion required for binding to the glycosaminoglycans was lost during this step. In most of the

endostatin batches that we tested, the addition of 5 μM zinc chloride resulted in a 35–50% increase in binding to heparin and heparan sulfate. However, we observed a much higher increase in binding in some endostatin preparations, up to 175% in the presence of zinc and up to 91% in the presence of calcium. This could indicate that loss of the divalent cation (likely to be zinc, as discussed below) does vary from one preparation to another and could explain the lack of endostatin binding to heparin in some experimental conditions. Indeed, mouse and human endostatin (a concentration of up to 2 μM) fail to bind, or bind only weakly, to heparin-albumin in solution, although both bound to a heparin column (7). The variation in zinc content could also account, at least in part, for the contrasting results and lack of reproducibility regarding the biological activities of endostatin, which have been attributed to incorrect folding and/or to differential post-translational modification between endostatins from different sources.

The requirement for a divalent cation in endostatin binding to heparin seems at odds with the report that heparin binding to endostatin is not affected by the loss of zinc binding (7). However, it should be noted that: (i) this result was obtained by mutagenesis to suppress the zinc binding site and not directly by adding ion chelator to inhibit the interaction as we did; and (ii) Sasaki *et al.* (7) used murine endostatin, whereas we used the human protein in this study. This latter difference might be of importance because variable zinc coordination occurs in murine endostatin (30).

Several cations, including Zn^{2+}, Ca^{2+}, and Mn^{2+}, are able to enhance the interaction. Because zinc is a constituent of human endostatin in solution and is present in a 1:1 molar ratio (11, 18), we assume that the cation required *in vivo* for binding to heparin or heparan sulfate is zinc. The depletion of divalent cations from immobilized heparin and heparan sulfate by injection of 10 mM EDTA prior to endostatin injection does not result in any significant change in binding, suggesting that the cation is associated with endostatin rather than with the glycosaminoglycan chains. The rate of the dissociation phase of the complexes formed between endostatin and heparin or heparan sulfate decreases in the presence of divalent cations, suggesting that they might stabilize the complexes. The increased binding of endostatin to itself observed by SPR in the presence of zinc is consistent with the existence of zinc-dependent dimers as observed in crystals of human endostatin (18).

The addition of zinc to endostatin was not required either for the anti-angiogenic activity of endostatin from 293-EBNA cells in a model of angiogenesis induced by VEGF or for its anti-proliferative activity on tumor cells and on endothelial cells stimulated by VEGF. This suggests that these two biological activities of endostatin are not mediated by its interaction with heparan sulfate when VEGF is the stimulating growth factor. The lack of effect of added zinc on the biological activities of endostatin elicited by VEGF is consistent with the fact that endostatin mutants with no zinc binding are still able to block the migration of endothelial cells induced by VEGF (12) and to inhibit tumor growth (12, 31).

In contrast to the results obtained with VEGF, the addition of zinc to endostatin enhances its anti-proliferative activity on endothelial cells stimulated by FGF-2. This suggests that when FGF-2 is used to stimulate cell proliferation, the anti-proliferative activity of endostatin is mediated, at least *in vitro*, by its binding to heparan sulfate. Our results support the existence of two different mechanisms (heparin-dependent and heparin-independent) for the anti-proliferative activity of endostatin depending on the growth factor used to induce cell proliferation.

The importance of heparin binding for the anti-angiogenic activity of endostatin also remains controversial. As for cell proliferation, it is likely that endostatin exerts its anti-angiogenic activity, at least *in vitro*, by two mechanisms, depending on the growth factor used to induce angiogenesis. Our data and those reported by Yamaguchi *et al.* (12) show that endostatin inhibits VEGF-induced angiogenesis independently of its ability to bind heparin. On the other hand, heparin binding is required for the inhibition of FGF-2-induced angiogenesis in the chicken chorioallantoic membrane (7, 13).

Recombinant human endostatin from 293-EBNA cells inhibits to a similar extent the proliferation of endothelial cells induced by VEGF and of the HT29 colon adenocarcinoma cell line. The fact that human endostatin is able to inhibit the proliferation of a tumor cell line is in agreement with the finding that murine endostatin inhibits the growth of C51 and HT29 cell lines (32). Endostatin might exert an anti-proliferative effect only on particular tumor cell lines, because murine endostatin produced in *Escherichia coli* has been reported not to inhibit the proliferation of Lewis carcinoma cells (1). Another point that deserves attention is that human endostatin inhibits the proliferation of a human (HT29) but not of a murine (C51) colon adenocarcinoma cell line. Species specificity regarding the effect of endostatin has also been reported for the *ex vivo* rat aortic ring assay (33).

In conclusion, endostatin is involved in a number of intermolecular interactions with the constituents of the extracellular matrix and also with membrane receptors such as integrins (34, 35). This indeed complicates studies aimed at determining the extent to which the interaction of endostatin with the heparan sulfate chains of the cell surface contributes to its biological activities. We are currently studying the multimolecular complexes that are located at the surface of endothelial cells and contain endostatin and its partners (heparan sulfate chains, integrins, and matrix metalloproteinase-2), to understand how they interact with each other and whether these interactions are involved in the anti-angiogenic activity of endostatin.

Acknowledgments—We thank Rabia Sadir for heparin and heparan sulfate oligosaccharides, John Gallagher and Malcolm Lyon for their generous gift of selectively desulfated heparins, and David J. S. Hulmes for critical reading of the manuscript.

REFERENCES

1. O'Reilly, M. S., Boehm, T., Shing, Y., Fukai, N., Vasios, G., Lane, W. S., Flynn, E., Birkhead, J. R., Olsen, B. R., and Folkman, J. (1997) *Cell* **88,** 277–285
2. Ramchandran, R., Karumanchi, S. A., Hanai, J., Alper, S. L., and Sukhatme, V. P. (2002) *Crit. Rev. Eukaryotic Gene Expression* **12,** 175–191
3. Marneros, A. G., and Olsen, B. R. (2001) *Matrix Biol.* **20,** 337–345
4. Sasaki, T., Hohenester, E., and Timpl, R. (2002) *IUBMB Life* **53,** 77–84
5. Ren, B., Hotin N., Rabasseda, X., Wang, Y. Z., and Wu, M. (2003) *Methods Find. Exp. Clin. Pharmacol.* **25,** 215–224
6. Sasaki, T., Fukai, N., Mann, K., Gohring, W., Olsen, B. R., and Timpl, R. (1998) *EMBO J.* **17,** 4249–4256
7. Sasaki, T., Larsson, H., Kreuger, J., Salmivirta, M., Claesson-Welsh L., Lindahl, U., Hohenester, E., and Timpl, R. (1999) *EMBO J.* **18,** 6240–6248
8. Karumanchi, S. A., Jha, V., Ramchandran, R., Karihaloo, A., Tsiokas, L., Chan, B., Dhanabal, M., Hanai, J. I., Venkataraman, G., Shriver, Z., Keiser, N., Kalluri, R., Zeng, H., Mukhopadhyay, D., Chen, R. L., Lander, A. D., Hagihara, K., Yamaguchi, Y., Sasisekharan, R., Cantley, L., and Sukhatme, V. P. (2001) *Mol. Cell* **7,** 811–822
9. Kreuger, J., Matsumoto, T., Vanwildemeersch, M., Sasaki, T., Timpl, R., Claesson-Welsh, L., Spillmann, D., and Lindahl, U. (2002) *EMBO J.* **21,** 6303–6311
10. Blackhall, F. H., Merry, C. L., Lyon, M., Jayson, G. C., Folkman, J., Javaherian, K., and Gallagher, J. T. (2003) *Biochem. J.* **375,** 131–139
11. Boehm, T., O'Reilly, M. S., Keough, K., Shiloach, J., Shapiro, R., and Folkman, J. (1998) *Biochem. Biophys. Res. Commun.* **252,** 190–194
12. Yamaguchi, N., Anand-Apte, B., Lee, M., Sasaki, T., Fukai, N., Shapiro, R., Que, I., Lowik, C., Timpl, R., and Olsen, B. R. (1999) *EMBO J.* **18,** 4414–4423
13. Dixelius, J., Larsson, H., Sasaki, T., Holmqvist, K., Lu, L., Engström, A., Timpl, R., Welsh, R., and Claessen-Welsh, L. (2000) *Blood* **95,** 3403–34011
14. Ricard-Blum, S., Bernocco, S., Font, B., Moali, C., Eichenberger, D., Farjanel, J., Burchardt, E. R., van der Rest, M., Kessler, E., and Hulmes, D. J. (2002) *J. Biol. Chem.* **277,** 33864–33869
15. Amara, A., Lorthioir, O., Valenzuela, A., Magerus, A., Thelen, M., Montes, M., Virelizier, J. L., Delepierre, M., Baleux, F., Lortat-Jacob, H., and Arenzana-Seisdedos, F. (1999) *J. Biol. Chem.* **274,** 23916–23925

16. Sadir, R., Baleux, F., Grosdidier, A., Imberty, A., and Lortat-Jacob, H. (2001) *J. Biol. Chem.* **276,** 8288–8296
17. Lyon, M., Rushton, G., Askari, J. A., Humphries, M., and Gallagher, J. (2000) *J. Biol. Chem.* **275,** 4599–4606
18. Ding, Y. H., Javaherian, K., Lo, K. M., Chopra, R., Boehm, T., Lanciotti, J., Harris, B. A., Li, Y., Shapiro, R., Hohenester, E., Timpl, R., Folkman, J., and Wiley, D. C. (1998) *Proc. Natl. Acad. Sci. U. S. A.* **95,** 10443–10448
19. Berman, H. M., Westbrook, J., Feng, Z., Gilliland, G., Bhat, T. N., Weissig, H., Shindyalov, I. N., and Bourne, P. E. (2000) *Nucleic Acids Res.* **28,** 235–242
20. Waldherr-Teschner, M., Goetze, T., Heiden, W., Knoblauch, M., Vollhardt, H., and Brickmann, J. (1992) in *Advances in Scientific Visualization* (Post, F. H., and Hin, A. J. S., eds) pp 58–67, Springer-Verlag, Heidelberg
21. Morris, G. M., Goodsell, D. S., Halliday, R. S., Huey, R., Hart, W. E., Belew, R. K., and Olson, A. J. (1998) *J. Comput. Chem.* **19,** 1639–1662
22. Imberty, A., Bettler, E., Karababa, M., Mazeau, K., Petrova, P., and Pérez, S. (1999) in *Perspectives in Structural Biology* (Vijayan, M., Yathindra, N., and Kolaskar, A. S. eds) pp 392–409, Indian Academy of Sciences and Universities Press, Hyderabad
23. Mulloy, B., Forster, M. J., Jones, C., and Davies, D. B. (1993) *Biochem. J.* **293,** 849–858
24. Clark, M., Cramer, R. D. I., and van den Opdenbosch, N. (1998) *J. Comput. Chem.* **8,** 982–1012
25. Vittet, D., Prandini, M. H., Berthier, R., Schweitzer, A., Martin-Sisteron, H., Uzan, G., and Dejana, E. (1996) *Blood* **88,** 3424–3431
26. Vittet, D., Buchou, T., Schweitzer, A., Dejana, E., and Huber, P. (1997) *Proc. Natl. Acad. Sci. U. S. A.* **94,** 6273–6278
27. Féraud, O., Cao, Y., and Vittet, D. (2001) *Lab. Investig.* **81,** 1669–1681
28. Parrish, R. F., and Fair, W. R. (1981) *Biochem. J.* **193,** 407–410
29. Hohenester, E., Sasaki, T., Olsen, B. R., and Timpl, R. (1998) *EMBO J.* **17,** 1656–1664
30. Hohenester, E., Sasaki, T., Mann, K., and Timpl, R. (2000) *J. Mol. Biol.* **297,** 1–6
31. Sim, B. K. L., Fogler, W., Zhou, X. H., Liang, H., Madsen, J. W., Luu, K., O'Reilly, M. S., Tomaszewski, J. E., and Fortier, A. H. (1999) *Angiogenesis* **3,** 41–51
32. Dkhissi, F., Lu, H., Soria, C., Opolon, P., Griscelli, F., Liu, H., Khattar, P., Mishal, Z., Perricaudet, M., and Li, H. (2003) *Hum. Gene Ther.* **14,** 997–1008
33. Kruger, E. A., Duray, P. H., Tsokos, M. G., Venzon, D. J., Libutti, S. K., Dixon, S. C., Rudek, M. A., Pluda, J., Allegra, C., and Figg, W. D. (2000) *Biochem. Biophys. Res. Commun.* **268,** 183–191
34. Rehn, M., Veikkola, T., Kukk-Valdre, E., Nakamura, H., Ilmonen, M., Lombardo, C., Pihlajaniemi, T., Alitalo, K., and Vuori, K. (2001) *Proc. Natl. Acad. Sci. U. S. A.* **98,** 1024–1029
35. Wickstrom, S. A., Alitalo, K., and Keski-Oja, J. (2002) *Cancer Res.* **62,** 5580–5589

Characterization of Endostatin Binding to Heparin and Heparan Sulfate by Surface Plasmon Resonance and Molecular Modeling: ROLE OF DIVALENT CATIONS

Sylvie Ricard-Blum, Olivier Féraud, Hugues Lortat-Jacob, Anna Rencurosi, Naomi Fukai, Fatima Dkhissi, Daniel Vittet, Anne Imberty, Bjorn R. Olsen and Michel van der Rest

J. Biol. Chem. 2004, 279:2927-2936.
doi: 10.1074/jbc.M309868200 originally published online October 28, 2003
